Sizing Individual Au Nanoparticles in Solution with Sub-Nanometer Resolution

Sean R. German,[†,‡] Timothy S. Hurd,[‡] Henry S. White,[*,†] and Tony L. Mega[*,‡]

[†]Department of Chemistry, University of Utah, Salt Lake City, Utah 84112, United States and [‡]Revalesio Corporation, 1200 East D Street, Tacoma, Washington 98421, United States

ABSTRACT Resistive-pulse sensing has generated considerable interest as a technique for characterizing nanoparticle suspensions. The size, charge, and shape of individual particles can be estimated from features of the resistive pulse, but the technique suffers from an inherent variability due to the stochastic nature of particles translocating through a small orifice or channel. Here, we report a method, and associated automated instrumentation, that allows repeated pressure-driven translocation of individual particles back and forth across the orifice of a conical nanopore, greatly reducing uncertainty in particle size that results from streamline path distributions, particle diffusion, particle asphericity, and electronic noise. We demonstrate ~0.3 nm resolution in measuring the size of nominally 30 and 60 nm radius Au nanoparticles of spherical geometry; Au nanoparticles in solution that differ by ~1 nm in radius are readily distinguished. The repetitive translocation method also allows differentiating particles based on surface charge density, and provides insights into factors that determine the distribution of measured particle sizes.

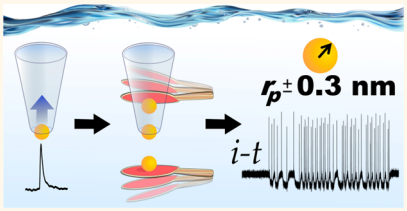

KEYWORDS: nanopore · Coulter method · resistive-pulse analysis · particle sizing · nanoparticles

Nanoscale particles are ubiquitous. They are found naturally as proteins, viruses, and vesicles, and they are produced synthetically for myriad applications from solar energy conversion to cancer therapeutics. The unique properties of nanoparticles important for their various functions arise from their size, charge, shape, material composition, and surface chemistry.[1] Comprehensive understanding of how these factors influence nanoparticle properties is important to the development of many fields, yet a high-resolution method for characterization of nanoparticle size in bulk solution is lacking. In this report, we describe a means of measuring particle size in solution with a resolution below 1 nm.

Dynamic light scattering (DLS) and electron microscopy (EM) are the most frequently used techniques for characterization of nanoparticles, but are limited in their usefulness. EM provides an exceptional size resolution of ~0.2 nm for particles removed from solution and placed under vacuum, but has yet to be used routinely for particles in solution.[2] DLS is an ensemble measurement commonly used to measure particle size and charge in bulk solution, and is well suited for monodisperse systems. But its ability to resolve peaks of multimodal distributions is controversial[3−5] and a resolution of particle size ratios below 3:1 is often questioned. Furthermore, DLS accuracy suffers increasingly with reductions in particle concentration and/or size (particularly below ~20 nm).[6] Nanoparticle Tracking Analysis (NTA) has recently gained popularity and is based on tracking the 2D diffusion rate of individual particles spending a sufficient length of time in the plane of observation. Under ideal conditions, particle size analysis by DLS and NTA both can be accurate to 2%, but heterogeneous samples can have errors an order of magnitude larger.[7]

Resistive pulse sensing has garnered significant attention over the past decade as a nanoparticle characterization system. On the basis of the Coulter principle,[8,9] the technique makes use of transient interruptions of conductance through a nanopore or nanochannel. The amplitude, duration, and frequency of the resistive pulse provide information about the particle size, charge, and concentration, respectively. Hundreds or thousands of particles are typically studied to gather statistics for an entire dispersion. The measurements of the size or charge of an individual particle, however, are generally associated with relatively large errors.

* Address correspondence to tmega@revalesio.com, white@chem.utah.edu.

Received for review April 1, 2015 and accepted June 17, 2015.

Published online June 17, 2015
10.1021/acsnano.5b01963

An individual particle translocation is a stochastic process in which the pulse amplitude depends upon the path taken through the pore[10−12] and also on the angle of rotation for aspherical particles.[10,13] Additionally, the duration or width of the pulse is randomly affected by diffusional motion of the particle. To reduce errors in nanopore-based DNA sequencing, Gershow *et al.* advocated recapture and trapping of individual molecules, dubbed molecular "ping-pong" to improve accuracy.[14] Reversal of particle direction based upon the translocation signal has been applied to polystyrene particles,[15,16] DNA,[14,17] dissolving bubbles,[15,18] and microorganisms,[15,19] providing information about particle diffusion, recapture rates,[14,16,17,20] bubble dissolution, viscosity effects, off-axial translocations, and aspherical particle orientation.[15,18] Both voltage and pressure switching have been used to reverse particle direction. Although Gershow *et al.*[14] raised the possibility, only Sen *et al.*[17] and Berge *et al.*[15] focused on repeated reversals of individual particles for the purpose of increasingly accurate characterization. Sen *et al.* involved high aspect ratio DNA particles, and Berge *et al.* studied various low aspect ratio microscale particles. There is a general need for high-resolution characterization of individual nanoparticles in their native solution state. Recent advances position resistive pulse sensing to address this problem.

Conical nanopores have unique advantages over rectangular nanochannels and cylindrical solid-state nanopores due to their ability to control nanoparticle dynamics, measure small particles, and significantly improve the probability that a particle "captured" from one side of the pore will be "released" back to that side by a return translocation.[20−23] In this report, we employ a conical nanopore in an automated pressure-reversal system that allows controlled trapping, and repeated translocations, of individual particles based on automated electronic triggering of the particle motion using the translocation pulses. This approach permits multiple observations of single particles, thereby improving measurement resolution to sub-nanometer levels traditionally associated with *ex situ* electron microscopy. We apply these methods to resolve the radii of individual Au nanoparticles to an unprecedented 0.3 nm size resolution, to detect subtle differences in the surface charge of particles, and to gain a better understanding of the intrinsic variability in resistive pulse sensing.

RESULTS AND DISCUSSION

We previously detailed the origin of the forces acting on charged nanoparticles in conical nanopores: electrophoresis (EP), electroosmosis (EO), and forces due to applied pressure, and demonstrated that the simultaneous application of external pressure and voltage can be used to precisely control particle velocity.[21] We have built on this past work to control the motion of

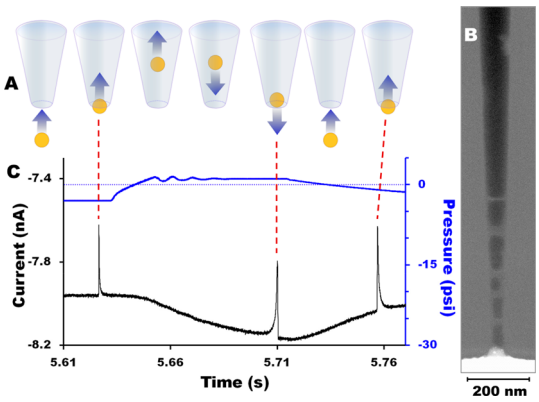

Figure 1. (A) Illustration of nanoparticle motion during particle reversal experiments. (B) Cross-sectional image of a glass nanopore obtained by FIB/SEM. The image is of a section parallel to the pore axis including the pore opening where salt has accumulated during the drying process. (C) Plot of current (black trace) and differential pressure (blue trace) *vs* time, showing three translocations of a nominally 59 nm radius particle. The initial current value at 5.61 s represents an open pore held constant at −300 mV applied potential. When −3 psi is applied (corresponding to a lower pressure within the capillary relative to the external solution), the solution is pulled into the capillary, resulting in a particle passing through the pore sensing zone at 5.63 s. The translocation pulse triggers a reversal of the pressure to 1 psi which is sufficient to force the same particle back out of the pore at 5.71 s, triggering a second reversal of pressure. This process of passing the particle back and forth through the pore can be continued indefinitely until the particle is lost by diffusion or the experiment terminated. The approximate mirror symmetry in the shapes of alternating resistive pulses reflects a particle entering and exiting the conical-shaped pore. The current baseline falls and rises with the pressure swings as described in the text.

individual particles in driving them back and forth through the orifice of a conical nanopore. Figure 1A shows a schematic drawing of the basic measurement concept, depicting a nanoparticle drawn from the bulk solution across the nanopore orifice (*i.e.*, the "sensing zone") and then, at a controlled time following the resistive pulse, the direction of fluid flow is reversed driving the particle back into the bulk solution. In the current experiments, the magnitude of the applied pressure is the dominant factor influencing particle motion as it is kept relatively large compared to the electrokinetic forces (EP and EO). Under these conditions, applying a negative pressure pulls a particle into the capillary through the sensing zone, while applying positive pressure releases the particle back out of the capillary. A unique feature of these experiments is that the translocations immediately trigger a reversal in the applied pressure. Rapid pressure reversal upon detection of a particle is important to ensure that the same particle translocates back and forth through the pore multiple times.

The process of particle reversal within the conical nanopore is illustrated in Figure 1A for the analysis of a 59 nm Au nanoparticle; an EM image of a glass nanopore cross section is shown in Figure 1B. Although the

pore in the TEM image is not the same one used for the trapping experiments reported here, it was fabricated by the same capillary pull-and-melt process.[21] Imaging nanopores of this type is a significant challenge because of the difficulty of locating the pore opening.[24−26] Importantly, the geometry in the image confirms the ∼2° cone angle estimated by independent size threshold measurements in German *et al.*[20] for pores prepared by the same method (Supporting Information Figure S1).

Figure 1C shows the measured current under −300 mV applied potential (black trace) and pressure changes (blue trace), which correspond to the particle motion illustrated in Figure 1A. The resistive pulse at 5.63 s indicates a particle passing into the pore from the external solution as the result of a differential pressure of −3 psi (lower pressure within the capillary relative to the external solution). The current pulse has an asymmetric shape, decreasing sharply as the particle approaches the pore orifice from the bulk solution and increasing back to the open pore current more slowly as the particle moves up into the conical nanopore. The change in resistance due to particle translocation is detected in real time and, within ∼20 ms of the translocation, the direction of fluid flow is reversed using LabVIEW software and an automated electronic system to increase the pressure to +1 psi within the capillary causing the particle to reverse direction. The particle then passes through the pore in the opposite direction as indicated by the asymmetric translocation pulse at 5.71 s, which has a shape that is the mirror image of the preceding pulse. The particle translocation continues to trigger pressure reversals resulting in additional translocations (*e.g.*, 5.76 s). The gradual fall and rise of the current baseline with the pressure swings has been noted before.[27,28] These slow baseline oscillations arise from a combination of ion current rectification and slightly different salt concentrations on either side of the pore due to evaporation (on the order of an ∼1% concentration difference).

Significantly, the precision in estimating the particle size and other characteristics based on pulse height and width improve as the number of back-and-forth translocation cycles increases. To achieve multiple measurement cycles that allow sub-nanometer size resolution, we designed the system shown in Figure 2 that encloses the capillary-based nanopore within a chamber in which the pressure is held constant by a proportional valve electronic pressure regulator. A dual proportional valve electronic differential pressure regulator is referenced to the chamber pressure, and allows both positive and negative pressure to be applied within the capillary to within ±0.0008 psi. By monitoring the slope of the *i*−*t* trace, we are able to trigger the reversal of pressure from positive to negative, and *vice versa*, upon detection of a translocation event. Electronic triggering allows multiple resistive

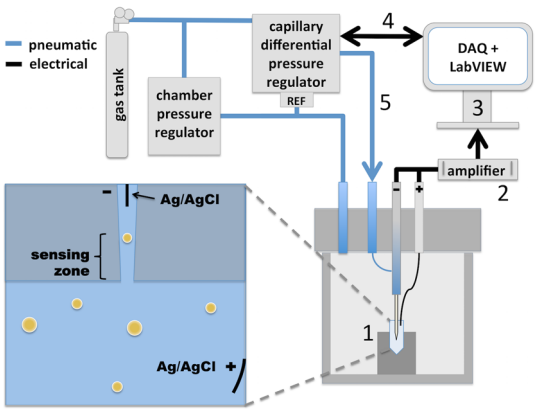

Figure 2. Automated particle trapping and sizing system. The glass nanopore and solution containing the particles (1) are placed inside a pressurized custom-built chamber. A pressure regulator controlling the chamber pressure is referenced to a dual proportional valve differential pressure regulator; the latter rapidly increases or decreases the pressure inside the capillary-based nanopore relative to the outer chamber. The cycle of events for moving the nanoparticle back and forth across the nanopore orifice are as follows: (1) a particle translocation event occurs; (2) the resulting resistive pulse is amplified and the *i*−*t* trace is passed to a DAQ card; (3) a LabVIEW program monitors the slope of the trace to detect the event; (4) a signal to the electronic regulator reverses the sign of the differential pressure; and (5) after a delay of ∼20 ms, the direction of fluid flow is reversed forcing the particle in the opposite direction back through the sensing zone. This process is repeated until sufficient measurement cycles are obtained to determine the particle size, or the particle is lost by diffusion. In the experiments reported here, typically 20−70 cycles are repeated to determine particle size.

pulse measurements on the same nanoparticle. As shown below, typically between 20 and 70 translocation cycles are performed on each particle.

In these experiments, we worked with well-characterized spherical Au nanoparticles of two different radii. For the larger particle size, two different surface charges were also studied (one with a carboxylated and one with a methylated polymer coating) in order to assess the effect of particle charge. TEM images of the larger radius particles in their dried state were analyzed with ImageJ software (see Supporting Information Figure S2). Upon the basis of images of 1700 particles, the particle size distribution was determined to be 59 ± 3 nm (±1σ). Application of standard error of the mean (SEM = $\sigma/\sqrt{N}$) gives a 99.7% confidence interval, or ±3 SEM, that the mean radius is 59.0 ± 0.2 nm. Resistive pulse sensing does not allow direct absolute measurement of a particle's size at high resolution. Therefore, we calibrated our nanopore system by assigning the mean radius derived from TEM images to the percent current blockade of the mean particle size resulting from hundreds of resistive pulse measurements on the same particles dispersed in solution. Each different nanopore needs to be calibrated in this way because of uncertainties in the pore size and geometry. Trapping experiments were performed in numerous pores, but unless specified, the

data presented in this paper is derived from experiments using a single ~80 nm radius nanopore (details for determining pore radii can be found in the Methods section). On the basis of measurements of 250 particles in a 1 M NaCl solution with 0.1% Triton X-100 at pH 7.2, 59 nm radius Au nanoparticles translocating through this pore gave an average percentage current blockade (%Δi) of 4.5%, where Δi is defined as the change in current due to the transient particle blockade relative to the baseline current. Since the resistive pulse height is proportional to the volume of electrolyte excluded by the translocating particle,[29]

$$\%\Delta i = k r_p^3 \quad (1)$$

where k is a proportionality constant relating %Δi to the nanoparticle radius, r_p. The value of k determined using the 59 nm radius Au nanoparticles, k = 4.5%/(59 nm),[3] was then used to measure the radius of a second nanoparticle of different size based upon its resistive pulse height (using the same pore). The direct relation of particle volumes to resistive pulse heights has been shown to hold within ~2% as long as the particle/pore diameter ratio is below 0.8.[24] To confirm measurements took place in this linear regime, the pores used for this work were etched successively wider (in dilute, buffered hydrofluoric acid while under an applied pressure of 5 psi as described in German *et al.*[21]) and additional resistive pulse traces were collected between etches for two particles of different radii (33 and 59 nm). We observed that the ratio of resistive pulse heights for the two particle sizes reaches a constant value for pores greater than 80 nm (Supporting Information Figure S3), justifying the use of eq 1.

%Δi values can be readily determined to with 0.1% (*vide infra*) by measuring the resistive pulse height for repeated translocations of the same nanoparticle, allowing its radius to be determined with a precision *of less than 1 nm*. Of course, the absolute accuracy in determining the particle size depends on the calibration of the resistive pulse magnitudes using the TEM-measured value of the average radius as the calibration standard equated to the mean of the resistive pulse measurements, which in this case has a standard error of the mean of ~1 nm.

The second Au particle size used in this study had a nominal radius of 33 nm, as determined by TEM (Supporting Information Figure S2). Resistive pulse sensing of a solution containing these nanoparticles yielded an average percent current blockade ~1/6 as large as that of the 59 nm particles, consistent with the predicted value of 0.17 (~1/6) based on eq 1. Figure 3A shows the $i-t$ trace for a resistive pulse measurement performed in a solution containing both 59 and 33 nm radius Au nanoparticles; in this representative trace, three individual Au nanoparticles were trapped and their radii measured over a time period of 25 s.

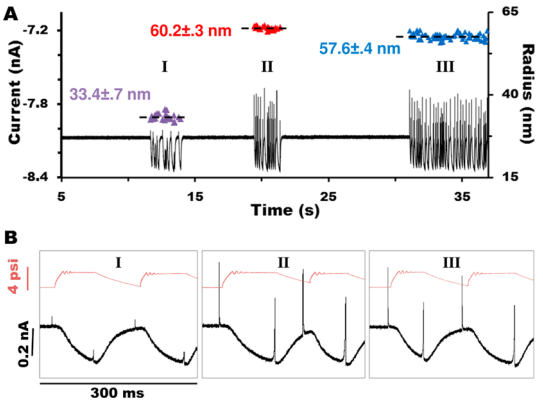

Figure 3. Trapping and analysis of particle size in a solution containing both 33 and 59 nm radius Au nanoparticles. (A) A section of an $i-t$ trace showing relatively long periods of open pore current, interdispersed by three particle trapping and size-measurement cycles. (B) Expanded $i-t$ trace from each trapping event in (A) showing two sets of forward and reverse translocations. The current baseline falls and rises with the pressure swings as described in the text. Measurements were made in a 1 M NaCl, pH 7.2, solution containing 0.1% Triton X-100, using a nanopore with an ~80 nm radius orifice. The particle radius calculated by a volumetric relationship from the resistive pulse heights (see text) is shown as individual points in (A); the dashed line and numerical value correspond to the average radius calculated for each particle. Confidence intervals of 99.7% are provided in each case, representing 3 times the standard error of the mean based on 24, 21, and 62 size-measurement cycles of the three particles, respectively.

Because the particle concentration is fairly low (10^9 particles/mL), there are relatively long stretches of time during which the open-pore current is measured while applying a negative pressure inside the nanopore. However, once a particle enters the pore, it ping-pongs back and forth through the sensing zone at a frequency of ~10 s^{-1} until it is manually ejected or is lost due to recapture failure, as discussed below. For the $i-t$ trace shown in Figure 3A, the first, second, and third particle made 24, 21, and 62 cycles, respectively, of passing back and forth through the sensing zone. The study of each of these specific particles was terminated when the particle diffused away from the pore. While the $i-t$ trace in Figure 3A appears complex, the expanded view of the $i-t$ trace for each particle, shown in Figure 3B, shows well resolved forward and reverse translocations.

The particle radii calculated from each translocation event using eq 1 are plotted directly above each corresponding peak in Figure 3A, along with the group mean. Each grouping of events can unequivocally be distinguished from another grouping as representing a new particle with a different mean radius. Repeated measurement of the resistive pulse peak height allowed the radii to be calculated as 33.4 ± 0.7, 60.2 ± 0.3, and 57.6 ± 0.4 nm (3 SEM based upon 24, 21, and 62 measurements, respectively).

Figure 4 demonstrates unprecedented size resolution afforded by the resistive pulse technique. In this

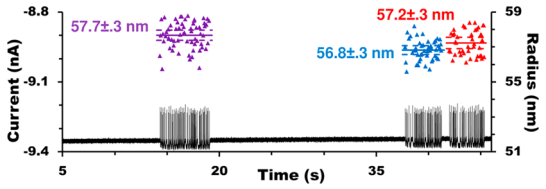

Figure 4. Trapping and analysis of particle sizes in solution containing 59 nm radius carboxylated Au particles. Section of an *i*−*t* trace showing periods of open pore current interdispersed by three particle trapping and size-measurement cycles. The radii calculated from the % current blockade is plotted above each translocation event. Each solid line represents the mean size and the dashed line represents 3 standard errors from the mean (3 SEM based upon 62, 47, and 43 measurements). Measurements were made in a 1 M NaCl, pH 7.2, solution containing 0.1% Triton X-100 using a ~95 nm radius pore calibrated using eq 1 where $k = 1.7\%/(59\ \text{nm})^3$.

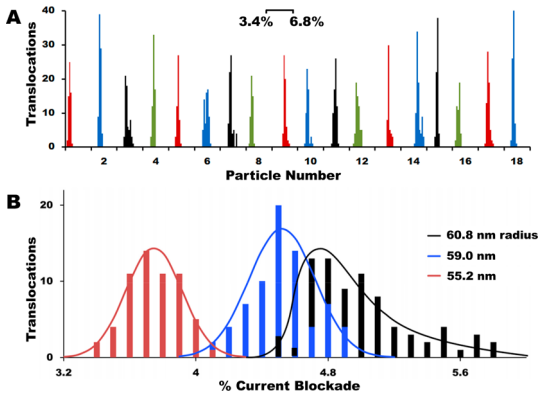

Figure 5. (A) Histograms of the percentage current blockade in which 59 nm radius particles were trapped and between 45 and 70 translocation cycles were recorded for each particle. Representative histograms for 18 different nanoparticles are shown, binned at 0.2% intervals to make the line widths visible. The intervals along the *x* axis correspond to a range of percentage current blockades between 3.4 and 6.8% for each individual particle. (B) Expanded view of the distributions for 3 different particles binned at 0.1% intervals (corresponding to particles 1, 2, and 3 in part A). The blue and red lines are Gaussian distribution fits; the black line is drawn to guide the eye. The distribution widths represent contributions from off-axial translocation and particle asphericity.

30 s trace, three particles that differ in absolute size by less than 1 nm are sequentially captured and each undergo 40−60 translocation reversals. Statistical averaging of the pulse heights allow their radii to be determined as 57.7 ± 0.3, 56.8 ± 0.3, and 57.2 ± 0.3 nm (3 SEM based upon 62, 47, 43 measurements).

The improved size resolution offered by this technique depends on the factors needed to achieve a sufficient number of particle reversals. To begin the sequence, a translocation must exceed the detectable particle-to-pore size ratio for the particular nanopore system, which generally ranges between ~1.5 and 80%.[30] The end of a trapping sequence on a single particle can be caused by a number of circumstances other than diffusion of the particle away. Despite the particle concentration being kept low, a second particle can occasionally enter the pore, doubly triggering the pressure system such that the pressure does not reverse. Also, a particle that passes through the pore when the differential pressure is less than 0.1 psi can have a peak width at half-maximum several milliseconds long, in which case the rate of change in current is not large enough to trigger a reversal. This is particularly an issue when triggering on small resistive pulse amplitudes, because the slope detection system will false trigger on the baseline oscillations if the threshold is set too low. If a trapping sequence is successful in acquiring more than sufficient data for the needs of the study, researcher intervention may also terminate the experiment. In this study, a particle was lost at the end of a sequence of between 20 and 70 reversals due to diffusion, researcher intervention, trigger failure, or a second particle approximately 50%, 33%, 12%, and 5% of the time, respectively, based on capture and analysis of ~300 different nanoparticles. Adjusting the concentration, timing, and pressures used for trapping allows the researcher to control the effectiveness of particle capture.

The resistive pulse technique is generally described as a single particle technique. However, the source and magnitude of variability in measuring particle size based on individual translocation events is often neglected in analyses, because of the difficulty in repeating the measurement on the exact same particle. The distribution of resistive pulse amplitudes for a single particle represents a combination of complex stochastic phenomena. First, the nanoparticle translocates through the nanopore orifice at different radial distances from the pore axis, which has been theoretically shown to produce different blockade currents.[10] A 15% maximum spread in Δi is predicted for off-axial translocations of perfectly spherical nanoparticles. Second, numerical modeling also shows that the orientation of aspherical particles significantly influences the peak amplitude.[10,13,31] The Au nanoparticles used in our experiments are nominally spherical, but it is apparent from the TEM images (Supporting Information Figure S2) that some are slightly oblong. In one experiment, we collected $\%\Delta i$ histograms for ~200 particles with 59 nm radius, of which 18 representative examples are shown in Figure 5A. Figure 5B shows expanded views of $\%\Delta i$ histograms for three different particles. Clearly, two of the distributions are nearly symmetrical, while the third is markedly skewed. Approximately 1/3 of the particles trapped and analyzed exhibit a skewed distribution, and the widths of the distributions were significantly larger (25−40%) than the 15% maximum predicted for off-axial translocations of perfect spheres.[10] We propose that the 25−40% spread in Δi values provides information about particle asphericity, with the smaller Δi values representing the particle's major axis coincident with the pore axis, and the larger

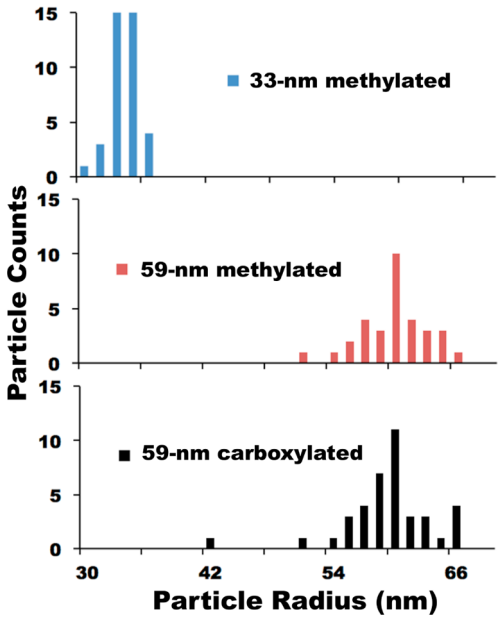

Figure 6. Histograms of the radii of ~40 particles from each particle type. Each count represents the mean radius determined from 20 to 70 translocation cycles of an individual particle. Particle sizes were measured in 1 M NaCl and 0.1% Triton X-100, pH 7.2, using an ~80 nm radius pore.

Δi values resulting as the particle's major axis and radial position departs from the pore axis.[10,31]

By measuring the radii of many individual nanoparticles, we can also determine the size dispersion of a collection of particles. Figure 6 shows the size histograms of the 33 nm radius methylated, 59 nm radius methylated, and 59 nm radius carboxylated Au nanoparticles, based on individual particle size measurements, each with sub-nanometer resolution. We believe the automated trapping and multiple translocation methodology described here can provide particle size distribution profiles at a resolution that has been hitherto unattainable in solution. Note that the widths of the size distributions (~5 nm for the 33 nm radius Au nanoparticles, and ~10 nm for the 59 nm radius Au nanoparticles) are much larger than the 0.3−0.7 nm precision in measuring individual particle sizes. Thus, because the variability in single particle radii is significantly less than the ensemble distribution widths, the distributions shown in Figure 6 reflect the true distribution of particle sizes. An F-test comparing the variance of both the TEM and resistive pulse measurements of the 59 nm radius particles shows to a 95% confidence interval that the distributions are not different.

It has been previously demonstrated that the particle velocity increases linearly with increasing pressure.[27] The effect of electrical charge on a particle's velocity during translocation is also well understood.[9,21,22,32,33] The duration of the resistive pulse (measured by the peak width at half height) is governed by both the velocity of pressure driven flow as well as electrokinetic phenomena associated with the charged particle and nanopore. The electrokinetic forces are typically simplified as electrophoretic (EP) forces on the particle and electroosmotic flow (EO) within the pore. EO manifests as a plug flow of fluid arising from the counterions associated with the charged walls, whereas the EP is dependent upon the charge of the particle.[34] In our experiments, the glass nanopore has a negative surface charge, and therefore, the net excess of positive counterions in the electrical double layer, under the influence of negative potentials, drag fluid into the pore by EO toward the cathode. Both the methylated and the carboxylated Au nanoparticles used in our experiments are negatively charged (DLS measured zeta potentials in deionized water yield −12 and −18 mV for the 33 and 59 nm radius methylated particles, and −35 mV for the 59 nm carboxylated particles, respectively. Zeta potential measurements could not be performed in higher NaCl concentrations, but the values would be expected to be much lower).

A particle's relative velocity through the nanopore due to the above forces is obtained from the duration of the resistive pulse, the latter measured as the reciprocal peak width at half-maximum. Figure 7A plots the relative velocity of an individual 60.3 ± 0.4 nm methylated and a 60.9 ± 0.3 nm carboxylated particle as a function of the differential pressure across the nanopore, while holding the applied voltage constant at −300 mV. Each set of data comes from trapping and repeated translocation of one particle at different pressures (34 and 42 measurements for the methylated and carboxylated particles, respectively). The tight grouping of reciprocal peak widths at positive pressures is a result of the differential regulator achieving its set point value quickly as the pressure is increased, causing each translocation exiting the pore to occur at nearly the same velocity. In our system, decreasing the differential pressure requires a longer time, and thus, the negative differential pressure value at which the particle returns into the pore has a greater variability, a consequence of the random diffusion of the particles. Figure 7A clearly illustrates that the velocity of the nanoparticle passing through the pore orifice is proportional to the instantenous differential pressure across the orifice at the moment of translocation. Figure 7A also shows that the additional electrophoretic force on the more highly charged carboxylated particle (red) results in a slight downward shift of the relative velocity *versus* pressure relationship. Because the applied potential is negative, the more highly negatively charged (red) particle exits the pore more quickly and enters the pore more slowly.

The *y*-intercepts of the linear fits to the data in Figure 7A, where the applied pressure is zero, reflect the relative velocity of the two particles resulting

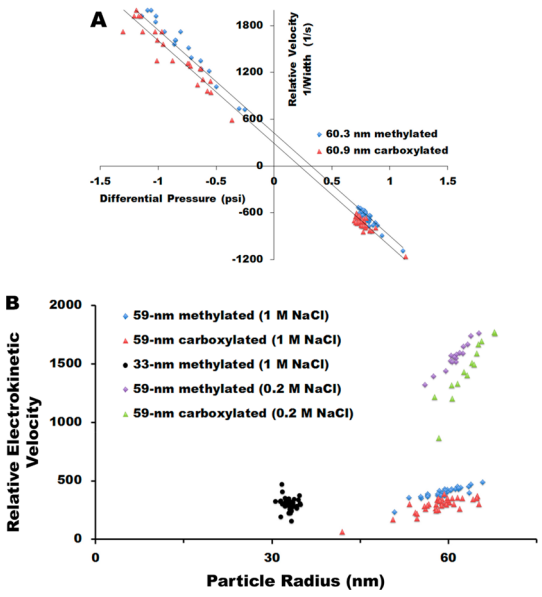

Figure 7. Relative nanoparticle translocation velocity *vs* differential pressure during a trapping sequence under −300 mV applied potential (pressure and voltage are external *vs* internal solution). (A) Data for a single 60.3 ± 0.4 nm methylated Au particle (blue diamonds) and an individual 60.9 ± 0.3 nm carboxylated Au particle (red triangles). Particles enter the pore under negative pressures and exit the pore under positive pressures. The *y*-intercept of the fitted line represents the particle velocity at zero applied pressure, and corresponds to the relative electrokinetic velocity. (B) Plot of relative electrokinetic velocities at −300 mV as a function of particle radius for individual particles in 0.2 and 1.0 M NaCl solutions demonstrating simultaneous determination of particle size and relative charge.

solely from electrokinetic forces. Both particles have a positive velocity (into the pore) in the absence of applied pressure because EO (directed into the pore) is the stronger electrokinetic force; however, the electrokinetic velocity is ∼25% slower for the more highly charge carboxylated particle due to stronger EP (directed out of the pore).

It has been demonstrated previously with resistive pulse sensing that both the size and charge of individual particles can be measured simultaneously.[9,22,33] In Figure 7B, we present size and relative electrokinetic velocity data collected with our particle trapping system. The results in Figure 7B were collected using the same nanopore (∼80 nm radius) in both 1.0 M NaCl and in 0.2 M NaCl for 33 nm methylated, 59 nm methylated, and 59 nm radius carboxylated spherical Au nanoparticles. Each data point represents a single particle that underwent between 20 and 70 translocation cycles to determine its mean radius and electrokinetic velocity (from the *y*-intercept of relative velocity *vs* differential pressure, as in Figure 7A for two particles). The data in Figure 7B suggest that the translocation velocity increases with particle size. The trend of increasing translocation velocity with particle size is not apparent for the smaller 33 nm radius particles. Also, lowering the electrolyte concentration to 0.2 M increases EO significantly and the trend with particle size becomes more pronounced. The trend disappears in a larger pore (∼95 nm radius) while still differentiating the charges of the two particles (Supporting Information Figure S4).

Manual control of applied pressure has also been used to recapture particles. Using conical glass nanopores, Lan *et al.* found that the probability of releasing a particle after translocation *into* the pore was >90% even with delays of 10 s before pressure reversal.[20] However, there is a significant difference in recapture probability for a particle that is confined inside the pore in comparison with a particle that is outside the pore. The fluid velocity falls off radially away from the pore opening and there is a characteristic distance away from the pore where the diffusional loss of the particle is much more probable than the fluidic velocity pulling the particle back to the pore. However, we have had marked success using pressure to control the motion. Particle recapture probability is governed by the response time of the system and by the magnitude of the forces applied toward retrieving the particle. Increasing the magnitude of the negative pressure serves to increase the characteristic distance, but can also have the detrimental effect of pushing the particle so quickly to the other side of the pore that the automated detection system may not have sufficient time to respond. Conical nanopores ameliorate this issue since recapture becomes almost certain while the particle is inside the pore. Hence, we are able to use a small positive pressure to retrieve the particle, which carries the particle a shorter distance away from the pore during the system response time after translocation out of the pore. This also allows the application of a large negative pressure for retrieving the particle outside the pore, thereby extending the characteristic recapture distance without any consequence of pushing the particle too far away after recapture into the pore. However, there is an upper bound on the range of pressures suitable for the technique, beyond which amplifier bandwidth limitations begin to underestimate peak heights due to excessive particle speeds.[27]

CONCLUSIONS

The basis of the resistive pulse technique lies in the size exclusion principle, and can be applied to biological and synthetic nanoparticles without any fundamental limitation. The single particle trapping and size measurement system based on differential pressure reversal upon particle detection represents a significant progression in resistive pulse sensing as a single particle characterization method. In addition to providing unprecedented sub-nanometer precision in particle size measurements, repeated measurements of resistive pulses will allow experimental testing of theoretical considerations of the variability inherent to

the method. The ability to trap and repeatedly characterize a single particle over a significant length of time also suggests the possibility of measuring the kinetics of subtle surface chemical reactions that result in a change in the size and/or electrical charge of a particle.

METHODS

Chemicals and Materials. Quasi-spherical Au nanoparticles with radii reported by the manufacturer of 33 nm ± 2% and 59 nm ± 2%, both conjugated with a methylated polymer, and 59 nm ± 2% radius conjugated with a carboxylated polymer were purchased from Nanopartz (Loveland, CO). Zeta potentials were measured as −12, −18, and −35 mV, respectively, in deionized water. Other materials included borosilicate glass capillaries (o.d. 1.5 mm, i.d. 0.86 mm, length 10 cm, Sutter Instruments), hydrofluoric acid (48%), ammonium fluoride solution (40%), sodium chloride, monosodium phosphate, disodium phosphate, Triton X-100, 0.25 mm silver wire (World Precision Instruments), 6 μm electroplated diamond on brass sanding disk (3M), nitrogen, hot glue, and household bleach (5% hypochlorite). Solutions were filtered through Millex-VV 0.1 μm syringe filters (Millipore).

Glass Nanopore. Fabrication of nanopores was as previously described[21] with the following modifications. Sanding of the terminal bulb was carried out above an inverted microscope (Olympus IX50 with an LMPlanFL 20×/0.40 objective) as the capillary was held by a micropositioner and pressed onto a diamond sanding disk rotated by a DC motor. The sanding was stopped just before the nanopore was opened and the capillary was immediately filled with 1.0 M NaCl. For hydrofluoric acid etching, an automated etching system was constructed to hold the capillary on a vertically oriented circular platform with stepper motor mounted to the shaft. A milled Teflon block with two wells containing electrodes was used to hold minimal amounts of 1:4 48% HF:40% NH_4F and NaCl solutions. An idler gear and second circular platform were positioned directly above the drive-mounted platform to ensure correct orientation of the capillary in the etchant and quenching solutions. The control system consisted of a microcontroller (Arduino Uno R3), high-speed stepper motor, and custom software to read the amplified signal from the 2273 PARSTAT potentiostat (Princeton Applied Research). Once a jump in the current indicated pore formation, the system immediately moved the capillary out of the etchant and into the NaCl solution in under 0.1 s. After forming a pore, capillaries were stored in a solution matching that inside the capillary. Pores were widened to the desired radius by etching further in 1:60 buffered hydrofluoric acid while applying a positive pressure of ∼5 psi across the pore. Between successive etches, resistive pulse measurements were made using Au nanoparticle standards. At a threshold size where approximately half of the particles pass through the pore and half block the pore entrance, we equate the pore radius to the particle radius, and calculate the nanopore's half cone angle by $R_p = 1/(\kappa r)[1/4 + 1/(\pi \tan \Theta)]$[35] where R_p is the resistance of the pore, r is the radius of the pore opening, κ is the solution conductivity, and Θ is the half cone angle. This same cone angle is used in calculating pore radii upon further etching.

Differential Pressure Particle Trapping System. A purpose built pressure chamber (Automated Systems, Tacoma) allowed electrical and pneumatic connection to a BNC style micropipette holder with a pressure port (QSW-B15P, Warner Instruments). Command signals from a custom LabVIEW program *via* an AD/DA (USB-6211, National Instruments) were sent to an electrically controlled proportional valve regulators (QPV1, Proportion Air) pressurized by a nitrogen tank. The program reads in voltage values from the resistive pulse amplifier at 10 kHz, calculating the slope of every ∼4 data points. Slopes exceeding a predefined threshold triggered the differential pressure switch. Detection cycles required less than 1 ms, although 1−5 ms delays were inserted to avoid duplicate detection of the same signal. The pressure response of the regulators was the factor limiting the detection cycle.

Resistive Pulse Sensing Measurements and Data Analysis. The $i-t$ traces and differential pressure were recorded using a HEKA EPC-10 USB amplifier at a cutoff frequency of 10 kHz applied with a three-pole Bessel low-pass filter. Patchmaster data acquisition software was used to collect and export raw data. A custom VBA Excel program was used to determine resistive pulse parameters. Each peak was inspected manually to ensure accurate measurements.

Conflict of Interest: The authors declare the following competing financial interest(s): Sean German, Timothy Hurd, and Tony Mega are employees of Revalesio Corporation.

Acknowledgment. The authors acknowledge S. Krämer for TEM imaging at the Materials Department of the University of California at Santa Barbara, and thank M. Edwards and J. Harris for helpful discussions. This work was supported by Revalesio Corporation and by AFOSR MURI FA9550-14-1-000.

Supporting Information Available: Detailed description of focused ion beam preparation of a nanopore lamella for TEM imaging is provided. TEM images of nanoparticles and their size analysis are discussed. Particle-to-pore size ratio effects are presented. Relative electrokinetic velocities in a larger pore are shown as well. The Supporting Information is available free of charge on the ACS Publications website at DOI: 10.1021/acsnano.5b01963.

REFERENCES AND NOTES

1. Murray, R. W. Nanoelectrochemistry: Metal Nanoparticles, Nanoelectrodes, and Nanopores. *Chem. Rev.* **2008**, *108*, 2688–2720.
2. Browning, N. D.; Bonds, M. A.; Campbell, G. H.; Evans, J. E.; LaGrange, T.; Jungjohann, K. L.; Masiel, D. J.; McKeown, J.; Mehraeen, S.; Reed, B. W. Recent Developments in Dynamic Transmission Electron Microscopy. *Curr. Opin. Solid State Mater. Sci.* **2012**, *16*, 23–30.
3. Rasteiro, M. G.; Lemos, C. C.; Vasquez, A. Nanoparticle Characterization by PCS: The Analysis of Bimodal Distributions. *Part. Sci. Technol.* **2008**, *26*, 413–437.
4. Ruf, H. Treatment of Contributions of Dust to Dynamic Light Scattering Data. *Langmuir* **2002**, *18*, 3804–3814.
5. Madani, H.; Kaler, E. W. Measurement of Polydisperse Colloidal Suspensions with Quasielastic Light Scattering. *Part. Part. Syst. Charact.* **1991**, *8*, 259–266.
6. Domingos, R.; Baalousha, M.; Ju-Nam, Y.; Reid, M.; Tufenkji, N.; Lead, J.; Leppard, G.; Wilkinson, K. Characterizing Manufactured Nanoparticles in the Environment: Multimethod Determination of Particle Sizes. *Environ. Sci. Technol.* **2009**, *43*, 7277–7284.
7. Filipe, V.; Hawe, A.; Jiskoot, W. Critical Evaluation of Nanoparticle Tracking Analysis (NTA) by NanoSight for the Measurement of Nanoparticles and Protein Aggregates. *Pharm. Res.* **2010**, *27*, 796–810.
8. Coulter, W. H. Means for Counting Particles Suspended in a Fluid. U.S. Patent. 2656508, October 20, 1953.
9. DeBlois, R. W.; Bean, C. P.; Wesley, R. K. A. Electrokinetic Measurements with Submicron Particles and Pores by the Resistive Pulse Technique. *J. Colloid Interface Sci.* **1977**, *61*, 323–335.
10. Qin, Z.; Zhe, J.; Wang, G.-X. Effects of Particle's Off-Axis Position, Shape, Orientation and Entry Position on Resistance Changes of Micro Coulter Counting Devices. *Meas. Sci. Technol.* **2011**, *22*, 045804.
11. Berge, L. I.; Jøssang, T.; Feder, J. Off-Axis Response for Particles Passing through Long Apertures in Coulter-Type Counters. *Meas. Sci. Technol.* **1990**, *1*, 471.
12. Stober, G.; Steinbock, L. J.; Keyser, U. F. Modeling of Colloidal Transport in Capillaries. *J. Appl. Phys.* **2009**, *105*, 084702.

13. Hurley, J. Sizing Particles with a Coulter Counter. *Biophys. J.* **1970**, *10*, 74–79.
14. Gershow, M.; Golovchenko, J. A. Recapturing and Trapping Single Molecules with a Solid-State Nanopore. *Nat. Nanotechnol.* **2007**, *2*, 775–779.
15. Berge, L. I.; Feder, J.; Jøssang, T. A Novel Method to Study Single-Particle Dynamics by the Resistive Pulse Technique. *Rev. Sci. Instrum.* **1989**, *60*, 2756–2763.
16. Schiel, M.; Siwy, Z. S. Diffusion and Trapping of Single Particles in Pores with Combined Pressure and Dynamic Voltage. *J. Phys. Chem. C* **2014**, *118*, 19214–19223.
17. Sen, Y.-H.; Jain, T.; Aguilar, C. A.; Karnik, R. Enhanced Discrimination of DNA Molecules in Nanofluidic Channels Through Multiple Measurements. *Lab Chip* **2012**, *12*, 1094.
18. Berge, L. I. Dissolution of Air Bubbles by the Resistive Pulse and the Pressure Reversal Technique. *J. Colloid Interface Sci.* **1990**, *134*, 548–562.
19. Boyd, C. M.; Johnson, G. W. Precision of Size Determination of Resistive Electronic Particle Counters. *J. Plankton Res.* **1995**, *17*, 41–58.
20. Lan, W.-J.; White, H. S. Diffusional Motion of a Particle Translocating Through a Nanopore. *ACS Nano* **2012**, *6*, 1757–1765.
21. German, S. R.; Luo, L.; White, H. S.; Mega, T. L. Controlling Nanoparticle Dynamics in Conical Nanopores. *J. Phys. Chem. C* **2013**, *117*, 703–711.
22. Kozak, D.; Anderson, W.; Vogel, R.; Chen, S.; Antaw, F.; Trau, M. Simultaneous Size and Z-Potential Measurements of Individual Nanoparticles in Dispersion Using Size-Tunable Pore Sensors. *ACS Nano* **2012**, *6*, 6990–6997.
23. Luo, L.; German, S. R.; Lan, W.-J.; Holden, D. A.; Mega, T. L.; White, H. S. Resistive-Pulse Analysis of Nanoparticles. *Annu. Rev. Anal. Chem.* **2014**, *7*, 513–535.
24. DeBlois, R. W.; Bean, C. P. Counting and Sizing of Submicron Particles by the Resistive Pulse Technique. *Rev. Sci. Instrum.* **1970**, *41*, 909–916.
25. Gao, C.; Ding, S.; Tan, Q.; Gu, L.-Q. Method of Creating a Nanopore-Terminated Probe for Single-Molecule Enantiomer Discrimination. *Anal. Chem.* **2009**, *81*, 80–86.
26. Li, G.-X.; Zhang, Z.-X.; Lin, X.-Q. Fabrication of Glass Nanopore Electrodes for Single-Molecule Detection of Beta-Cyclodextrin. *Chin. J. Anal. Chem.* **2010**, *38*, 1698–1702.
27. Lan, W. J.; Holden, D. A.; Liu, J.; White, H. S. Pressure-Driven Nanoparticle Transport Across Glass Membranes Containing a Conical-Shaped Nanopore. *J. Phys. Chem. C* **2011**, *115*, 18445–18452.
28. Vogel, R.; Anderson, W.; Eldridge, J.; Glossop, B.; Willmott, G. A Variable Pressure Method for Characterizing Nanoparticle Surface Charge Using Pore Sensors. *Anal. Chem.* **2012**, *84*, 3125–3131.
29. Lan, W.-J.; Holden, D. A.; Zhang, B.; White, H. S. Nanoparticle Transport in Conical-Shaped Nanopores. *Anal. Chem.* **2011**, *83*, 3840–3847.
30. Kozak, D.; Anderson, W.; Vogel, R.; Trau, M. Advances in Resistive Pulse Sensors: Devices Bridging the Void between Molecular and Microscopic Detection. *Nano Today* **2011**, *6*, 531–545.
31. Golibersuch, D. C. Observation of Aspherical Particle Rotation in Poiseuille Flow *via* the Resistance Pulse Technique. *Biophys. J.* **1973**, *13*, 265–280.
32. Steinbock, L. J.; Stober, G.; Keyser, U. F. Sensing DNA-Coatings of Microparticles Using Micropipettes. *Biosens. Bioelectron.* **2009**, *24*, 2423–2427.
33. Ito, T.; Sun, L.; Crooks, R. M. Simultaneous Determination of the Size and Surface Charge of Individual Nanoparticles Using a Carbon Nanotube-Based Coulter Counter. *Anal. Chem.* **2003**, *75*, 2399–2406.
34. Schoch, R.; Han, J.; Renaud, P. Transport Phenomena in Nanofluidics. *Rev. Mod. Phys.* **2008**, *80*, 839–883.
35. White, H. S.; Bund, A. Ion Current Rectification at Nanopores in Glass Membranes. *Langmuir* **2008**, *24*, 2212–2218.